Nuclear Engineering and Technology 57 (2025) 103545

Contents lists available at ScienceDirect

Nuclear Engineering and Technology

journal homepage: www.elsevier.com/locate/net

Original Article

Bi_2O_3 additive effects on gamma radiation shielding properties of $45SiO_2$-$20B_2O_3$-$23Na_2O_3$-9CaO-$3Al_2O_3$ glass

Mohammad Rezvani [a,*], Hossein Javid Ghezelgechi [a,b]

[a] Department of Materials Science and Engineering, University of Tabriz, Tabriz, 5166616471, Iran
[b] Department of Civil Engineering, Ozyegin University, Nisantepe, Orman Sk, Cekmekoy, Istanbul, 34987, Turkey

ARTICLE INFO

Keywords:
Glasses: x-ray diffraction: radiation damage
Infrared & Raman spectroscopy

ABSTRACT

Radiation poses a significant threat to living organisms, necessitating the development of effective shielding materials. This study investigates the properties of glass materials with varying proportions of SiO_2 and B_2O_3, selecting $45SiO_2$–$20B_2O_3$–$23Na_2O$–9CaO–$3Al_2O_3$ (mol%) as the base composition. X-ray diffraction analysis confirmed the amorphous nature of the prepared glasses, while differential thermal analysis (DTA) determined glass transition temperatures (Tg). Precise density measurements were conducted to validate the structural findings. Monte Carlo N-Particle (MCNP) simulations were employed to assess the photon energy absorbance characteristics of the glasses, revealing that adding Bi_2O_3, up to 15 mol% in the GSB2-15 glass, significantly enhances gamma-ray shielding properties. Key results show that increasing Bi_2O_3 content from 0 to 15 mol% improves photon energy absorption, with the GSB2-15 glass achieving a density of 2.691 g/cm^3 and a Tg of 533.19 °C, both superior to those of other compositions. Fourier Transform Infrared (FTIR) and Raman spectroscopy further demonstrated that GSB2-15 maintains structural stability under gamma radiation doses up to 3.98 Gy, with minimal bond disruption. These findings establish the GSB2-15 glass, with 15 mol% Bi_2O_3, as a highly effective candidate for radiation shielding applications.

1. Introduction

Radiation sources threaten human health and the integrity of sensitive equipment, necessitating effective shielding materials [1]. Exposure to X-rays, gamma rays, and neutrons impacts both the environment and living organisms [2].

Glass materials have garnered interest due to their broad applications, including space technology, optical waveguides, reactor inspection, and high-level nuclear waste (HLW) management [3]. Many researchers have studied ceramic composites for radiation shielding. For example, Kayrat et al. [4] investigated the gamma radiation shielding efficiency of radiation-resistant composite ceramics, evaluating the impact of composition variations and highlighting that the addition of TiO_2 enhances resistance to external influences and improves mechanical strength, or Daquan Shi et al. [5] evaluated the technical and gamma radiation shielding properties of sustainable ultra-high-performance geopolymer concrete (UHPGC) compared to normal concrete, finding that the gamma-ray shielding capacity of barite-enhanced UHPGC improved by 8.8 %. Polyvinyl alcohol (PVA) is also utilized as a radiation shielding material for low-energy radiation interactions. Polymer nanocomposite films have been studied by incorporating gadolinium into PVA, showing that increasing the gadolinium content enhances the linear absorption coefficient and mass attenuation coefficient [6]. While concrete materials and ceramics have been widely employed as radiation-shielding barriers in high-radiation environments, their utility is constrained by certain limitations. These drawbacks encompass issues such as reduced density, water loss, and susceptibility to cracking under the influence of high-energy radiation, leading to photon absorption. Additionally, the opacity of concrete walls presents challenges in radiation-centric applications, including research laboratories and medical equipment [7,8].

In recent years, there has been a remarkable upswing in the utilization of protective glasses to shield against extremely short-wavelength radiation encountered in space and radiation emanating from equipment used in medical, agricultural, and nuclear energy fields. Glass holds a unique advantage in its ability to remain transparent to visible light while offering a wide range of variability in chemical composition. The presence of continuous structures with robust chemical bonds is a critical characteristic of radiation materials. Several glass systems have been explored for their effectiveness in shielding against high-energy

* Corresponding author.
E-mail addresses: rezvani@tabrizu.ac.ir (M. Rezvani), hossein.javid@ozu.edu.tr (H. Javid Ghezelgechi).

https://doi.org/10.1016/j.net.2025.103545
Received 8 December 2024; Received in revised form 15 January 2025; Accepted 14 February 2025
Available online 1 March 2025
1738-5733/© 2025 Korean Nuclear Society, Published by Elsevier Korea LLC. All rights are reserved, including those for text and data mining, AI training, and similar technologies. This is an open access article under the CC BY-NC-ND license (http://creativecommons.org/licenses/by-nc-nd/4.0/).

Table 1
Compositions of glasses.

Composition (%mol) Sample code	SiO_2	B_2O_3	Na_2O	Al_2O	CaO	SiO_2/B_2O_3
GSB1	50	15	23	2	10	3.34
GSB2	45	20	23	2	10	2.25
GSB3	40	25	23	2	10	1.60

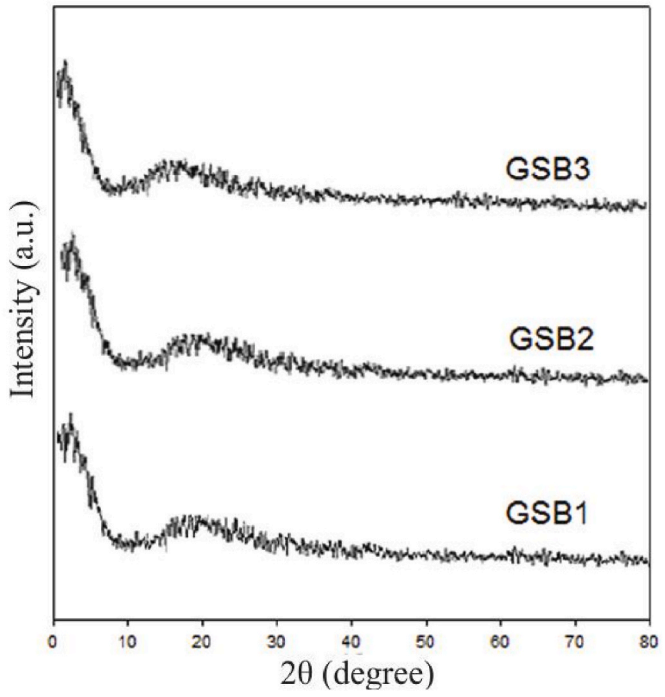

Fig. 1. XRD patterns of the GSB1, GSB2, and GSB3 glasses.

radiation, including silicate, borate, and barium glass systems.

Recent studies have highlighted the exceptional optical properties and radiation shielding capabilities of borate-based glasses, emphasizing their potential for advanced applications in medical and nuclear fields [9,10]. However, it is borosilicate glasses that enjoy widespread preference due to their exceptional attributes, such as a low thermal expansion coefficient (TEC) and impeccable chemical durability [11].

Introducing barium, lead, and bismuth oxides into glass compounds has demonstrated positive effects on their capacity to shield against gamma and X-ray radiation. The non-toxic nature of barium and bismuth renders them favorable alternatives to lead [2,12]. Recent studies have highlighted the potential of advanced glass systems, including those containing Bi_2O_3, to improve gamma radiation shielding, making them valuable for various applications in radiation protection [13,14]. Bismuth and lead share striking similarities in terms of atomic weight, ionic radius, and electronic configuration. Both elements outperform barium in the realm of high-energy radiation shielding [15]. Ghada ALMisned et al. [16]. demonstrated that incorporating Bi_2O_3 as a reinforcement significantly enhances the anti-nuclear radiation properties of Bi_2O_3-B_2O_3-BaO-ZnO composite glasses. Kirdsiri [17] suggests that bismuth and barium can potentially replace lead in the development of lead-free radiation-protecting glass, and this substitution could be effective at appropriate photon energy levels, reducing the environmental toxicity associated with lead. Also, Chanthima's study suggests that the addition of Bi_2O_3 in borophosphate glasses can be used for some applications such as radiation shielding glass due to the high density of these glasses [18]. Consequently, this study incorporates bismuth oxide into the base glass composition, capitalizing on its superior radiation absorption properties and non-toxic characteristics.

This study is significant as it identifies the optimal SiO_2 and B_2O_3 ratios and the precise addition of Bi_2O_3 to enhance gamma radiation shielding properties in borosilicate glasses. Unlike previous research, which primarily focused on conventional materials or limited compositions, this work explores Bi_2O_3-doped glasses in detail, combining experimental analyses such as X-ray diffraction(XRD), FTIR, and Raman, with MCNP and XCOM simulations. The findings highlight the superior shielding efficiency and structural stability of GSB2-15 glass, establishing it as a novel and environmentally friendly alternative to lead-based materials. This research contributes to advancing radiation shielding technologies for medical, nuclear, and aerospace applications.

2. Materials and methods

The glass composition chosen for this study, denoted as (65-x) SiO_2. xB_2O_3.$3Al_2O_3$.$9CaO$.$23Na_2O$ (where x = 15, 20, 25 mol%), is detailed in Table 1. The glasses resulting from these compositions were designated as GSB1, GSB2, and GSB3.

This specific glass composition for radiation shielding is a well-established choice in the field [2,19,20]. The glasses were prepared using the melt-quenching technique. A blend of high-purity B_2O_3 (directly) (99 %), Na_2CO_3 (99 %), $CaCO_3$ (99 %), Al_2O_3, and silica (SiO_2) was meticulously mixed and homogenized. To ensure the absence of bubbles in the melts, Sb_2O_3 (99.9 %) and As_2O_3 (99.9 %) were employed as refining agents. Boron and calcium oxides are known to promote phase separation in glass. However, based on the observed appearance of the samples, which are nearly transparent with no visible turbidity, it appears that phase separation is either absent or minimal. For a more detailed investigation, using an electron microscope or conducting a chemical resistance test may reveal separation at higher magnifications. Since the extent of separation did not significantly affect the gamma-ray absorption results, it was deemed negligible in the final analysis.Precise measurements were taken for each batch, and the mixtures were melted in zirconia crucibles, covered with alumina plates to regulate mass loss, in an electric furnace at 1200 °C, with a heating rate of 10 °C/min. The melting process extended for 1 h to achieve desirable homogeneity. The homogenized melts were subsequently poured into preheated stainless-steel molds of the required dimensions. These samples were promptly transferred to an annealing muffle, maintained at temperatures between 400 °C and 500 °C, depending on the glass system, for annealing over 3 h. Following an additional hour, the muffle was allowed to naturally cool to room temperature.

To confirm the amorphous nature of the glasses, XRD analysis was conducted using a Siemens D500 instrument. The density of the specimens was measured utilizing the Archimedes principle, and differential thermal analysis (DTA) curves were generated at a rate of 10 °C/min with a DTG-60AH Shimadzu instrument to determine the Tg. The density of the glasses was determined using distilled water as the immersion liquid on an electronic weighing balance machine [21]. Fourier transform infrared (FT-IR) transmittance spectra of the glass samples were recorded using a Bruker-Tensor27 FT-IR spectrophotometer, while the Raman intensity of the glass samples was measured with a Bruker-Senterra-2009 Dispersive Raman Microscope to assess structural changes before and after gamma irradiation at doses of 1.59 and 3.98 MGy (Gy = Gray = 1 J/kg).

Gamma irradiation was carried out using a 137Cs gamma cell (10 mCi) (CPN MC-S) and a 241AmBe (50 mCi) source at Tabriz University, Iran. To predict the photon energy absorption of the glasses following gamma irradiation, MCNP simulation software and the XCOM program were employed.

3. Result and discussion

3.1. Base glass composition selection

Borosilicate glasses can prevail over all the drawbacks of concrete

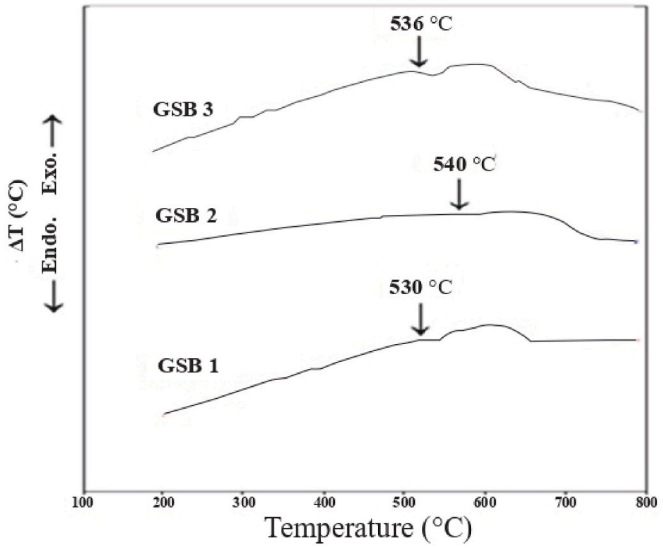

Fig. 2. Differential Thermal Analysis curves of the GSB1, GSB2, and GSB3 glasses.

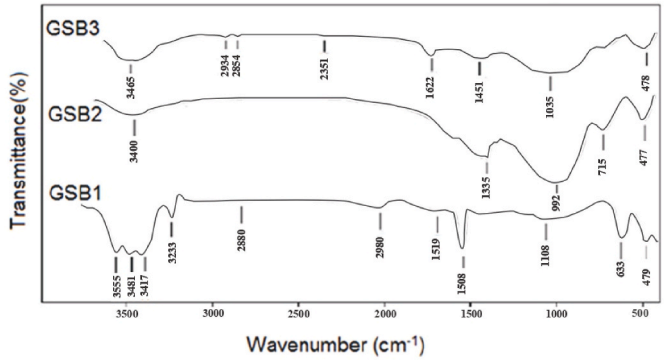

Fig. 3. FTIR spectroscopy of GSB1 (x = 15), GSB2 (x = 20), and GSB3 (x = 25).

materials with their high mechanical strength, high transparency, high chemical durability, and most importantly excellent radiation shielding behavior when compared to concrete materials [22,23].

Borosilicate glass is a leading choice for immobilizing HLW due to its exceptional radiation shielding properties and structural durability. This study focuses on SiO_2–B_2O_3-based glasses to explore their potential for enhanced shielding performance.

3.1.1. XRD patterns and DTA of the base glass

XRD patterns of the glasses are shown in Fig. 1. As illustrated in the patterns, there is no peak, indicating that no unfavorable crystallization has occurred throughout the preparation of the glass.

The T_g (a significant factor in survey structural) changes, because it is sensitive to density changes, bond type, hardness, and coordination number of network makers. Curves with different amounts of B_2O_3 are presented in Fig. 2. The Tg for glass GSB1 is about 530 (C°), which increases by increasing the amount of B_2O_3 in the composition and eventually drops again. By the decreasing of $\frac{SiO2}{B_2O_3}$ ratio from 3.34 to 2.25, boron coordination increases from three to four, and in this case, the number of tetrahedron units of BO_4 increases simultaneously, since the boroxol networks of BO_3 groups with a coordination number of three have lower bond strength than BO_4 groups with a coordination number of four, the T_g increased at first, then by $\frac{SiO2}{B_2O_3}$ ratio decreasing to 1.60 which causes coordination number reduction from four to three and also an increasing number of Non-Bridge Oxygens (NBOs), resulting T_g

Table 2
FTIR spectroscopy absorption bonds of (65-x) SiO_2. $xB_2O_3.3Al_2O_3.9CaO.23Na_2O$,
x = 15,20,25 %mol.
GSB1(x = 15), GSB2(x = 20), GSB3(x = 25)
[19, 28, 29].

Wave number (cm^{-1})	Absorption bands
477-478-479	Bending vibrations of B-O-B rings
633	bending vibrations of Si-O-Si
715	bending vibrations of O_3B-O-BO_3 and twisted vibrations of borates
922	stretching vibrations of B-O bonds in $[BO_4]$ units of tetra and Penta borate B_3O_5, $B_6O_8^-$, $B_8O_{18}^{2-}$
1035–1068	- stretching vibrations of B-O bonds in $[BO_4]$ units of tetra and Penta borate B_3O_5, $B_6O_8^-$, $B_8O_{18}^{2-}$ - overlapping contributions of borate and silicate groups, including $[BO_4]$ and $[BO_3]$ - asymmetric stretching vibrations of B-O bonds in trigonal $[BO_3]$ units - stretching vibrations of B-O bonds in $[BO_3]$ units such as Penta, pyro, meta borate chains, and rings
1451	- Asymmetric vibrations of B-O bonds in $[BO_3]$ and BQ_2O^- units
1508	asymmetric stretching vibrations of B-O bonds in $[BO_3]$ units - stretching vibrations of B-O bonds in $[BO_3]$ units such as Penta, pyro, meta borate chains, and rings
1619–1622	asymmetric stretching vibrations of B-O bonds in $[BO_3]$ units
>2000	Vibrations of molecular water BOH, OH, SiOH

Table 3
Glass composition with additives.

Composition (%mol) Sample code	SiO_2	B_2O_3	Na_2O	Al_2O_3	CaO	Bi_2O_3(excessive additive- grams per 100 g of Composition)
GSB2-5	45	20	23	3	9	5
GSB2-10	45	20	23	3	9	10
GSB2-15	45	20	23	3	9	15

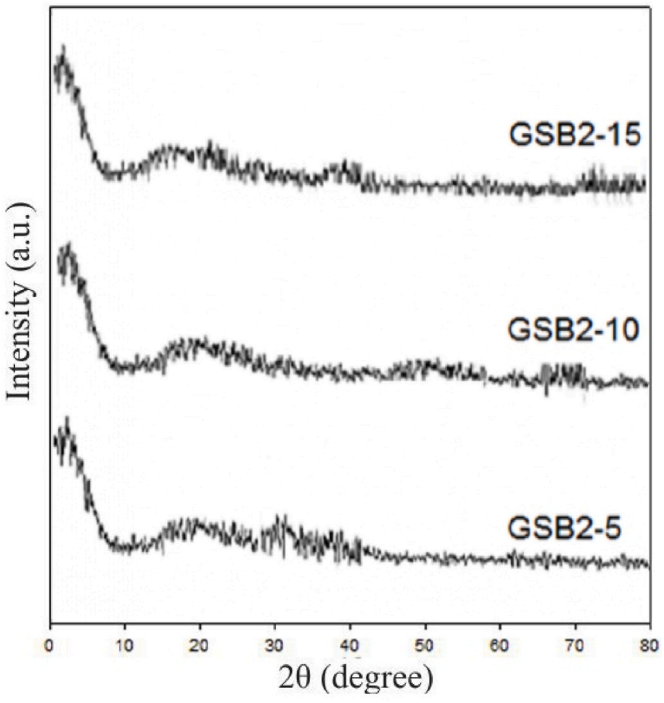

Fig. 4. XRD patterns of GSB2-5, GSB2-10, and GSB2-15 glasses.

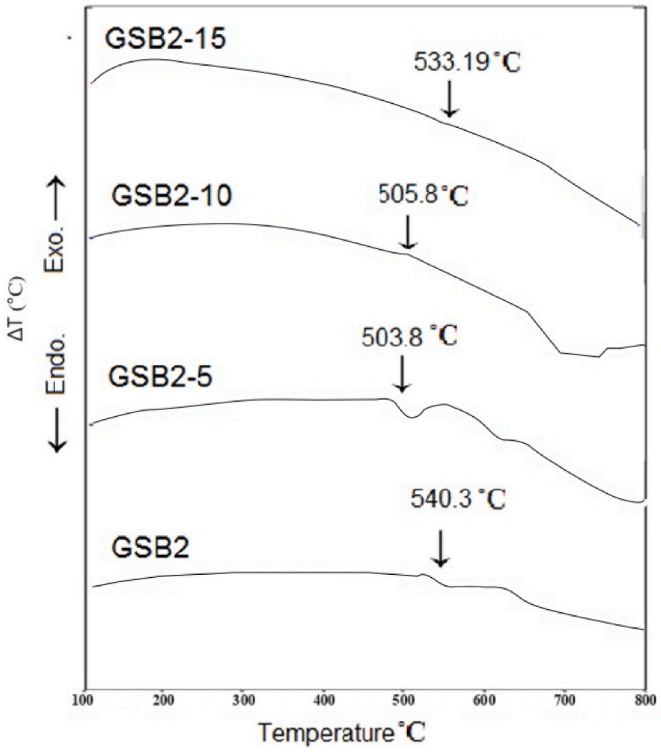

Fig. 5. DTA patterns of samples with different amounts of Bi_2O_3.

Table 4
Density and T_g of the glasses.

Property Sample	D(g cm^{-1})	T_g(° C)
GSB2	2.707	540.3
GSB2-5	2.544	503.8
GSB2-10	2.582	505.8
GSB2-15	2.691	533.19

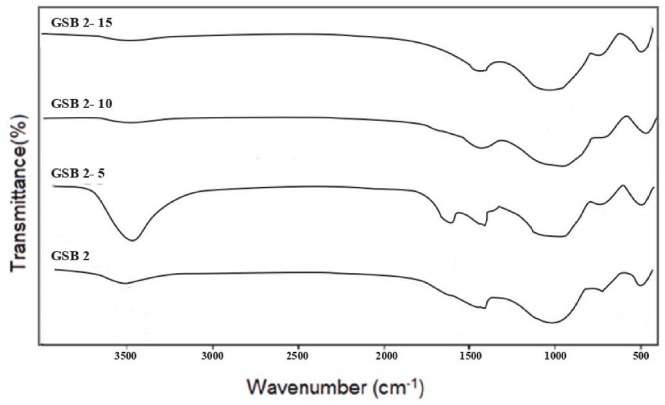

Fig. 6. FTIR spectra of GSB2- GSB2-15.

reduction.

3.1.2. FT-IR spectroscopy of glasses with different molar ratios (SiO_2/B_2O_3)

To investigate (65-x) SiO_2.xB_2O_3.3Al_2O_3.9CaO.23Na_2O glass, its FT-IR spectra in different frequencies for different borate and silicate structural groups have been analyzed as shown in Fig. 3. This FT-IR spectrum is divided into high-frequency and low-frequency ranges. The absorbance in the high-frequency region (1600-4000 cm^{-1}) is

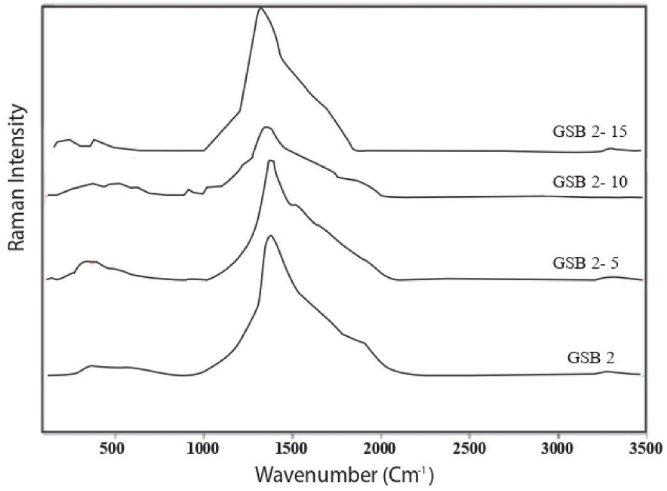

Fig. 7. Raman spectra of glasses with different Bi_2O_3 mol percent.

caused by inevitable moisture gained during the preparation of samples and is not helpful for the current study as it demonstrates gained moisture and does not impact the interpretation of the results [24].

Low-frequency ranges should be studied to identify the structure of the glasses [25–28]. With increasing amounts of B_2O_3 in the glass composition, absorption intensities increase; this is due to the increase of B-O-B bonds in the glass [28]. The absorption bonds are shown in Table 2. The absorption peak in 663 cm^{-1} is assigned to bending vibrations of Si-O-Si in glass with 15%mol B_2O_3, which is not observed in other glasses and is due to the reduction of Si-O-Si bonds and increase of B-O bonds with the rise of B_2O_3 content. In the glass containing 20 % mol B_2O_3, a distinct peak is observed, which can be attributed to the bending vibrations of O_3B-O-BO_3 and the twisted vibrations of borates. However, this particular peak is conspicuously absent in the glass with 25 % mol B_2O_3, suggesting that no new B-O links are formed in the latter composition. Furthermore, in the 20 % mol B_2O_3 glass, a notable absorption peak in the range of 990–1100 cm-1 is observed, which is associated with the stretching vibrations of B-O bonds within [BO_4] units of Tetra and Penta borate structures (B_3O_5, B_6O_8-, B_8O_{18}) [29]. This peak is characterized by its heightened intensity. Additionally, a distinct absorption peak at 1335 cm^{-1} is solely detected in the 20 % B_2O_3 glass and can be attributed to the B-O bonds present in [BO_3] units within penta and meta borates [30]. As the B_2O_3 content increases to 25 % mol, a new absorption peak emerges, signifying the creation of non-bridging oxygen species (NBOs).

According to the FTIR spectrum, it is evident that the glass system featuring 20 % mol B_2O_3 comprises tetrahedral structures of SiO_2 and tetrahedral BO_4 units, showcasing a more continuous arrangement. Consequently, it can be inferred that non-bridging oxygen species have not been generated in this particular glass composition. As a result, the GBS2 glass system is anticipated to exhibit superior radiation shielding properties.

3.1.3. GSB2 glass as a base composition of glasses

The GSB2 glass exhibits the highest density among the three glass systems, which can be attributed to the increase in boron oxide content. This increase leads to a reduction in non-bridging oxygens, thereby enhancing the connectivity of the glass network, particularly up to 20 % mol B_2O_3. Additionally, this glass also boasts the highest Tg. However, as the boron oxide content surpasses 20 % mol, the coordination number of boron within the B_2O_3 structure decreases from four to three, resulting in a decrease in both density and Tg in the GSB3 glass. Moreover, the analysis of the FTIR spectroscopy reveals that the glass system with 20 % mol B_2O_3 contains tetrahedral SiO_2 structures and tetrahedral BO_4 units, highlighting a more continuous arrangement. As a result, the

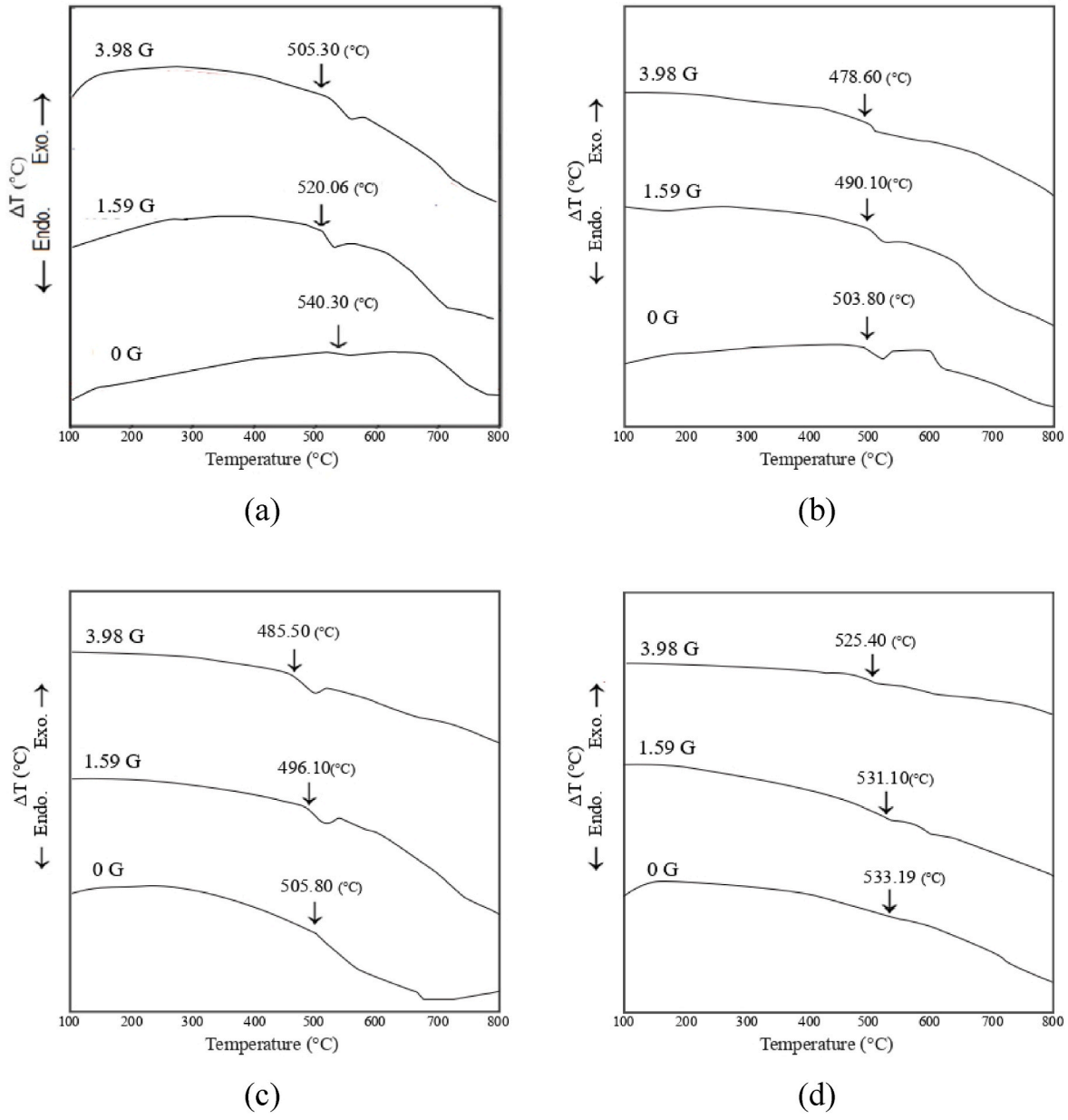

Fig. 8. DTA patterns of the glasses after gamma irradiation with the total dose of 1.59 (G), and 3.98 (G) a) GSB2 glass. b) GSB2-5 glass. c)GSB2-10 glass. d) GSB2-15 glass.

Table 5
T_g and ΔT of GSB2, GSB2-5, GSB2-10, and GSB2-15 glasses before and after 1.59 (G) and 3.98(G) dose gamma radiation.

Glass	Radiation Final Dose(G)	T_g (°C)	$\Delta T = T_{g2} - T_{g1}$
GSB2	0	540.30	0
GSB2	1.59	520.07	19.93
GSB2	3.98	505.30	35.00
GSB2-5	0	503.80	0
GSB2-5	1.59	490.10	13.70
GSB2-5	3.98	478.60	25.20
GSB2-10	0	505.80	0
GSB2-10	1.59	496.10	9.70
GSB2-10	3.98	485.50	20.30
GSB2-15	0	533.90	0
GSB2-15	1.59	531.10	2.80
GSB2-15	3.98	525.40	8.50

GBS_2 glass system is considered a more suitable candidate to serve as the base for radiation shielding glasses.

3.2. The properties of the glasses contain Bi_2O_3

The glass Compositions after the addition of different amounts of Bi_2O_3 are shown in Table 3 to assess the impact of Bi_2O_3 addition on glass features and radiation shielding properties.

3.2.1. The amorphous structure of the glasses in the presence of Bi_2O_3

As shown in Fig. 4, all XRD patterns of samples have no crystallization peaks, and bismuth oxide doesn't contribute to phase segregation (distinct regions or phases with different components within the glass matrix), nucleation, and crystal growth in any sample.

3.2.2. Thermal behavior and the density of the glasses in the presence of Bi_2O_3

The DTA patterns of the samples, incorporating varying quantities of

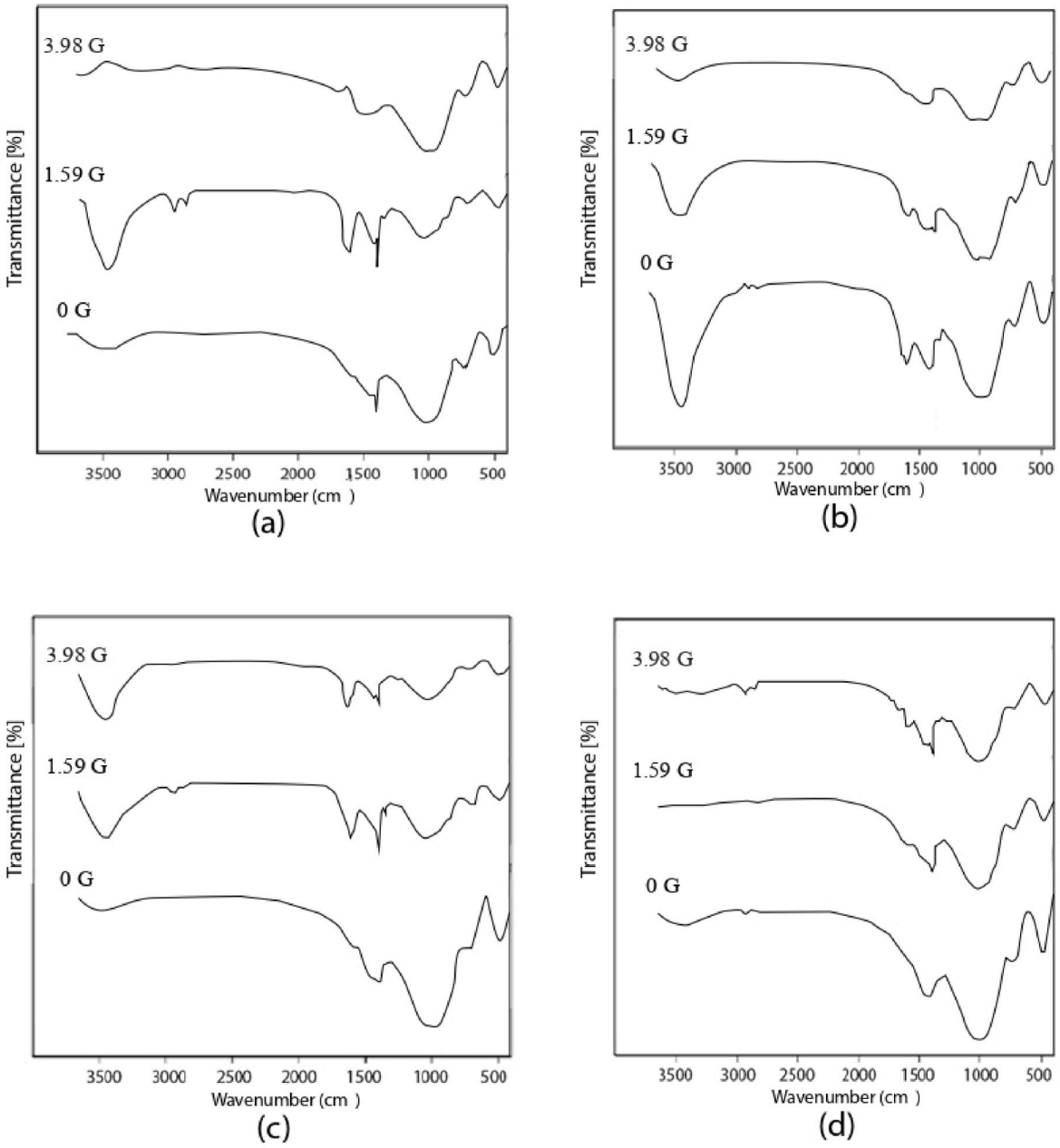

Fig. 9. FTIR spectroscopy of GSB2(a), GSB2-5(b), GSB2-10(c) and GSB2-15(d) glasses before and after 1.59(G) and 3.98(G) dose gamma radiation.

Bi_2O_3, are depicted in Fig. 5. The data illustrates that as the Bi_2O_3 content escalates from 0 to 10 % mol, there is a notable 35 °C reduction in the Tg. This reduction is primarily attributed to the lower melting point of bismuth, leading to an increased concentration of non-bridging oxygens (NBOs) and consequently diminishing the connectivity of the glass structure. Conversely, in the case of glass GSB2-15, a change in the coordination number of bismuth from 3 to 6 results in an improvement in structural connectivity, leading to a subsequent increase in the Tg.

The density and T_g of the glasses are shown in Table 4. With the increase of Bi_2O_3 from 0 to 15 %mol, at first, despite the high atomic mass of bismuth, in this glass, the role of this cation is as a modifier, leading to a significant increase in molar volume and a subsequent decrease in density so the structure of the glasses loosens, and T_g and density decrease, but after adding Bi_2O_3 up to 15 %mol, the effect of the increased mass on the volume is more pronounced, resulting in an increase in density and new structures formed and replaced previous ones in glass, so the density and T_g of glass increase again. In the glass GSB2-15, the density has been increased by about 0.109(g cm^{-1}), and T_g has been increased by about 27 °C in comparison to GSB2-10 glass.

3.2.3. FTIR investigation of glasses containing different amounts of Bi_2O_3

The FTIR spectra of GSB2- GSB2-15 glasses are shown in Fig. 6. The absorption peak in 1400–1500 cm^{-1} wavenumber is due to the vibrations of B-O bonds in BO_3 and the creation of NBOs [28]. For the GSB2-5 glass, this peak has high intensity, but for GSB2-15 has lower absorption intensity, and few NBOs are created; thus. By increasing Bi_2O_3 the intensity of absorption peak in 715 cm^{-1} wavenumber, which relates to Bi-O bonds [29,31,32], has been increased.

3.2.4. Raman spectroscopy of glasses with different amounts of Bi_2O_3

Raman spectra of glasses with different amounts of Bi_2O_3 are shown in Fig. 7. The bonds are seen in 495–505 cm^{-1} and 362 cm^{-1}, and are related to bending vibrations of Si-O-Si bonds [32]. The peak in 572 cm^{-1} is associated with Bi-O bonds in BiO_6 hexagonal [33], and their

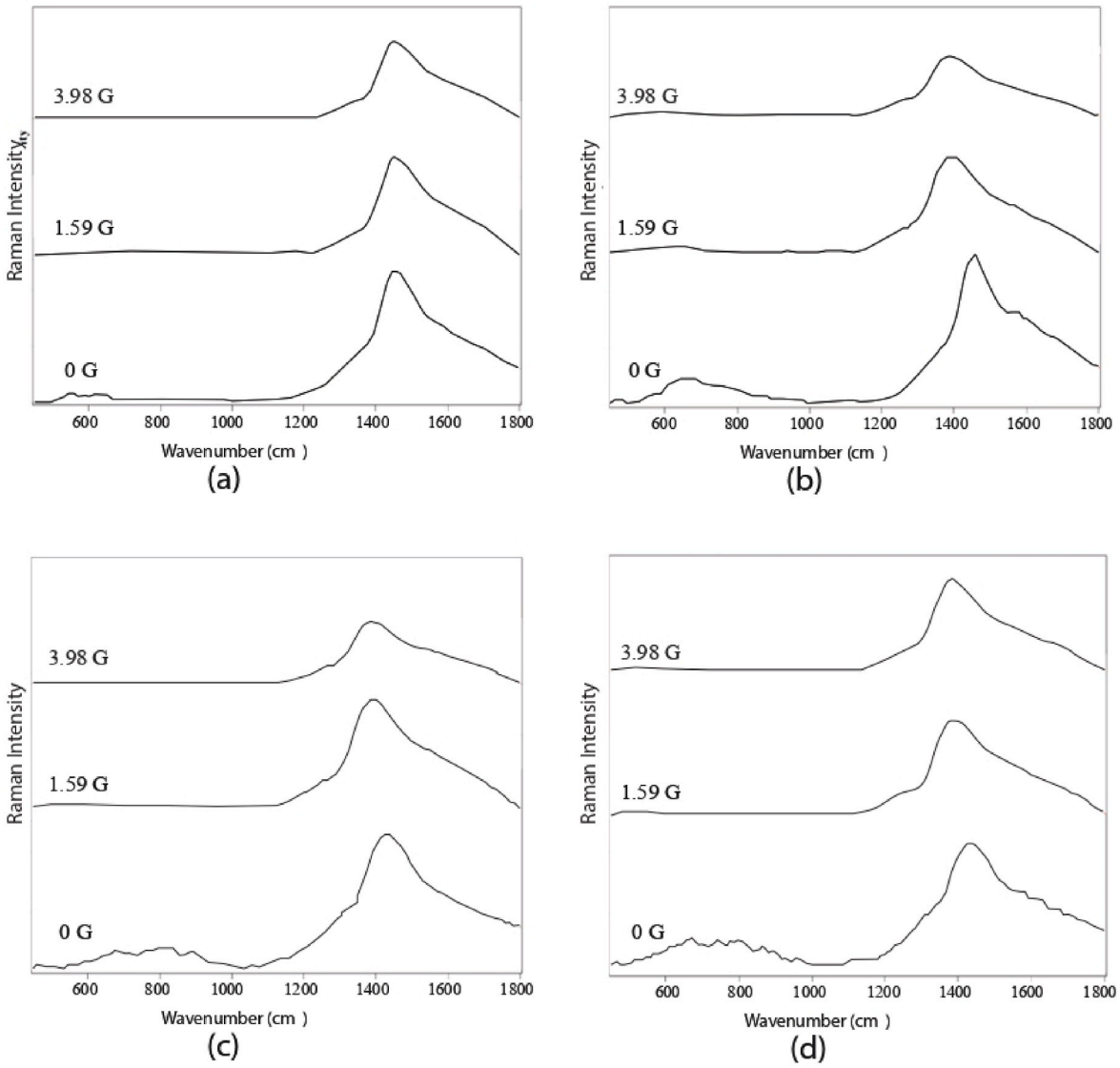

Fig. 10. Raman spectroscopy of the a) GSB2, b) GSB2-5, c) GSB2-10, and d) GSB2-15 glasses before and after gamma irradiation with the final dose of 1.59 and 3.98 (G).

number decreased with the increase in Bi_2O_3 content. The sharp rise in 1250–1320 cm^{-1} is due to the stretching vibrations of Bi-O bonds in BiO_3 pyramidal units. The intensity of the peak strengthens by increasing Bi_2O_3 content.

3.3. Gamma radiation effects on the glasses

The structural, physical, electrical, and optical properties of glass can be changed under radiation. X-ray and gamma-ray can cause defects such as segregation, fluorescence, and rupture of chemical bonds [3].

To investigate the effect of radiation on the structure of glasses, DTA, FTIR, and Raman spectroscopies were carried out on irradiated samples, and the radiation shielding property of glasses was tested and simulated by the XCOM program and MCNP code.

3.3.1. Gamma radiation dose calculation

For the glass $45SiO_2.20B_2O_3.3Al_2O_3.9CaO.23Na_2O$ containing Bi_2O_3 as an additive, the absorbed dose was calculated with Eq. (1):

$$D_{glass} = \frac{\mu - glass}{\mu - air} D_{air} \quad (1)$$

D = the absorbed dose, μ = mass attenuation coefficient, $D_{air} = 70.7$ (mSv/h)

The activities of 137Cs and AmBe as sources of Gamma radiation were 5.6209 G and 48 mci(1 ci = 3.7×10^7).[1]

$$D_{glass} = \frac{0.081\left(\frac{mSv}{h}\right)}{0.072\left(\frac{mSv}{h}\right)}$$

$$D_{glass} = 79.54\left(\frac{mSv}{h}\right)$$

$$Dose_{(in\ 20hrs)} = 79.54\left(\frac{mSv}{h}\right) \times 20(hr) \times \frac{1(sv)}{0.001\ (msv)} \times \frac{1(G)}{1sv} = 1.59(G)$$

$$Dose_{(in\ 50hrs)} = 79.54\left(\frac{mSv}{h}\right) \times 50(hr) \times \frac{1(sv)}{0.001\ (msv)} \times \frac{1(G)}{1sv} = 3.98(G)$$

[1] G = Gray = 1 J/kg.

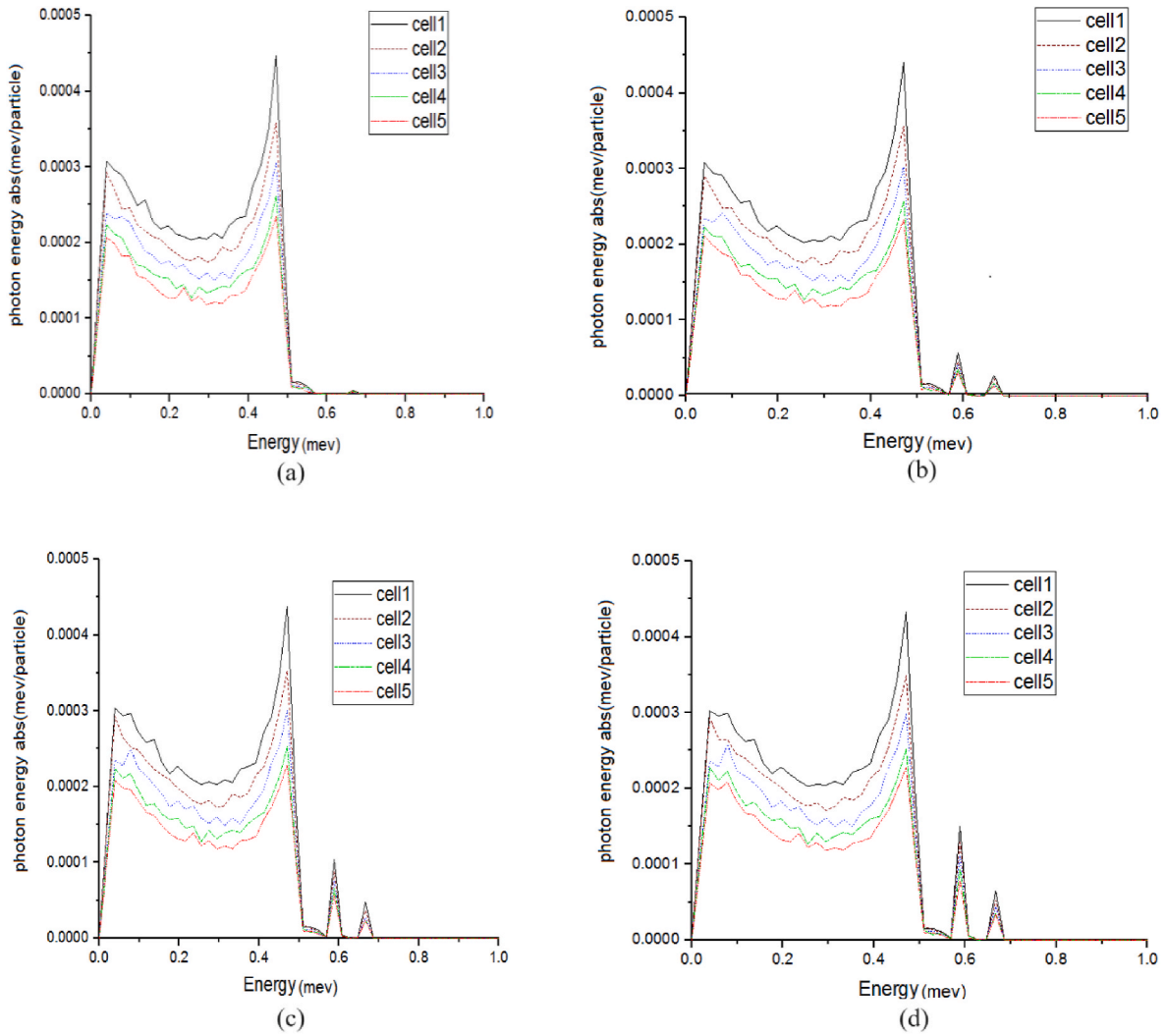

Fig. 11. Photon energy absorption of the a) GSB2, b) GSB2-5, c) GSB2-10, and d) GSB2-15 glasses.

Attained final dose of 1.59(G) in 20hrs and 3.98(G) in 50hrs.

3.3.2. *Gamma radiation effects on T_g of the glasses*

DTA patterns of the glasses after gamma irradiation with the total dose of 1.59 (G) and 3.98 (G) are shown in Fig. 8.

As can be seen in Fig. 8, and Table 5, the T_g of the glasses has been decreased because of bond rupture and glass structure failure after radiation. T_g of the GSB2-15 glass has changed slightly under the total doses of 1.59 and 3.98(G), which shows this glass has a good radiation shielding property under both doses.

3.3.3. *Gamma radiation effects on FTIR spectroscopy of the glasses*

To examine the glass structure changes, FTIR, and Raman spectrum were studied after radiation.

With Gamma radiation, several changes in glass structure occur, and absorption peaks start to widen, and their intensities decrease [34].

Fig. 9 shows the FTIR spectroscopy of the glasses under gamma irradiation with the final doses of 1.59(G) and 3.98(G). In the GSB2 glass, after gamma irradiation, peak intensity and wave number at 1100 (cm-1), which relates to the asymmetric stretching vibration of the Si-O-Si bond in the tetrahedral SiO_2, has been reduced, representing link break [19]. Frequency and intensity of absorption peaks between 1200-1400 (cm^{-1}) relate to B-O bond stretching vibration of BO_3 and BQ_nO^{-1} (relates to the borate groups where n shows the number of non-bridge oxygen) units from meta and orthoborate groups [28,35] and NBO stretching vibration of BO_3 units in penta, and metaborate rings [29] have been increased with radiation due to non-bridge oxygen creation and structure rupture.

Absorption peaks between 940 and 930 (cm^{-1}) relate to the B-O bond stretching vibration of BO unit in the triborate, tetraborate, and pentaborate groups [36], and absorption peaks around 1500 (cm^{-1}) relating to the stretching vibration of BO_3 groups [37] have been increased under gamma in GSB2-5 glass.

After gamma radiation, the intensity of the Si-O-Si bonds absorption peak in wave number 1030(cm^{-1}) and absorption peak in wave number about 1500 (cm^{-1}), which relates to the stretching vibration of BO_3 groups [37] has been increased in the GSB-10 Glass. The intensity of the absorption peak of Si-O-Si bonds in wave number 1030(cm^{-1}) has been decreased slightly after gamma irradiation in the GSB2-15 glass. It indicates that these bonds have been reduced less than the GSB2-5 and GSB2-10 glasses bonds under radiation. The absorption peak at wave number about 1500 (cm^{-1}) relates to the stretching vibration of BO3 groups [37]. It has been increased after radiation, but this is a minor increase compared to the absorption peak's rising in the GSB2-5, and GSB2-10 glasses after irradiation.

For the GSB2-10 glass under the final dose of 1.59(G), no significant reduction has occurred, but under the final dose of 3.98(G) intensity of these picks has been decreased. At least for the GSB2-15 glass, there was a significant reduction in the intensity of these picks only under gamma irradiation with the dose of 3.98(G), and this implies structural stability

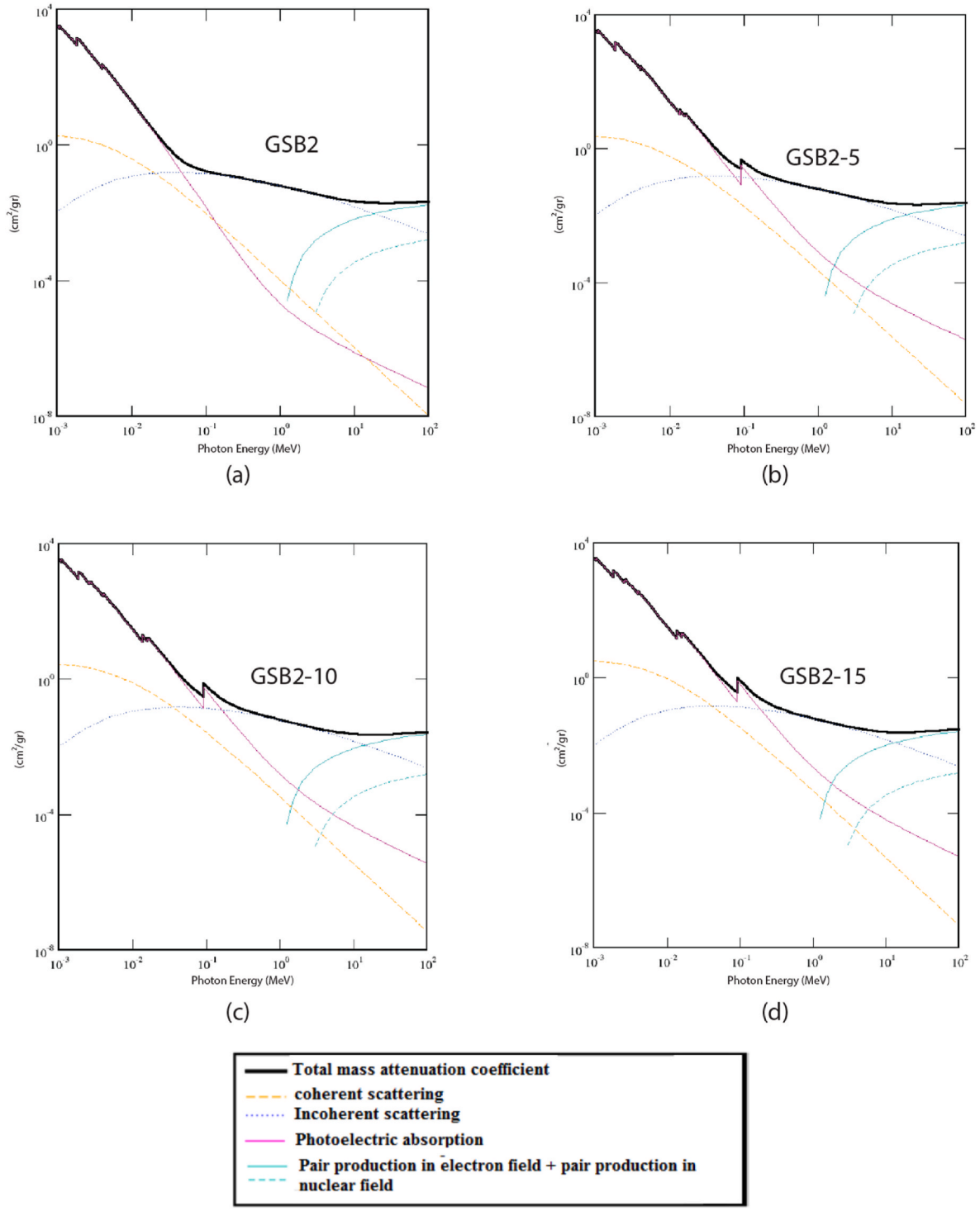

Fig. 12. Atomic absorption coefficient diagram based on photon energy by adding Bi_2O_3 in a) GSB2 b) GSB2-5 c) GSB2-10 d) GSB2-15 glasses.

of the GSB2-15 glass under high-energy radiation.

3.3.4. Gamma radiation effects on Raman spectroscopy

Fig. 10 shows Raman spectroscopy of the GSB2, GSB2-5, GSB2-10, and GSB2-15 glass before and after the final doses 1.59(G) and 3.98 (G) of gamma irradiation. The absorption peak at wave number 130(cm^{-1}) relates to the stretching vibration of Bi-O-Bi bonds in BiO3 and BiO_6 units, and the absorption peak at wave number 575(cm^{-1}) relates to the stretching vibration of Bi-O bonds in the hexagonal BiO_6 [33], the intensity of these picks has been dropped by gamma irradiation which indicates the loss of Bi-O bonds under irradiation. Still, this decrease is slighter in the GSB2-10 and GSB2-15 glasses.

The absorption peak at wave number 1250–1500 (cm^{-1}) relates to the stretching vibration of B-O-B and OB3-O-BO3 bonds in BO_3 units [19] for the GSB2-15 glass; there was a significant reduction in the intensity of these peaks which implies structural stability of the GSB2-15 glass under high-energy radiations.

3.3.5. Comparison with other glass systems

The changes in the Tg observed in GSB2-15 glass are attributed to

increased open sites within the glass structure, resulting from reduced bond cohesion that facilitates the reorganization of the glass matrix. However, these changes are less pronounced in GSB2-15 compared to commercial cobalt-doped glass, where FTIR bond alterations are also less significant in the former [38].

DTA, FTIR, and Raman analyses of boro-tellurite glasses modified with molybdenum and strontium oxide (with 35 % or 70 % molar substitution of TeO_2 for B_2O_3) show significant changes due to non-bridging oxygen formation when exposed to varying gamma doses. In contrast, GSB2-15 glass exhibits fewer structural changes, underscoring its superior gamma radiation shielding properties [39].

In our study, the FTIR analysis of irradiated GSB2-15 glass samples revealed no significant peak shifts or bond alterations. This stability aligns with observations in lead borate glasses, known for their excellent radiation shielding performance. The minimal change in FTIR peaks further confirms the reliability of GSB2-15 as an effective gamma radiation shielding material [40].

Overall, the incorporation of Bi2O3 into the glass composition enhances its gamma radiation attenuation capacity, positioning GSB2-15 as a promising candidate for radiation protection applications. Its performance is comparable to or superior to that of other advanced glass systems.

3.4. Radiation absorption simulation

To assess glass resistance against gamma radiation, MCNP, and XCOM program code was used.

3.4.1. Radiation absorption simulation of the glasses by MCNP code

To assess glass resistance against gamma radiation, MCNP code was used. To validate the simulations, we ensured that the MCNP input parameters, including material density, photon energy range, and glass composition, closely matched the experimental setup. Fig. 11 shows the photon energy absorption of the GSB2, GSB2-5, GSB2-10, and GSB2-15 glasses, all the cells have the same composition in each sample, and they have different geometry.

The results from MCNP and XCOM simulations showed good agreement, with both approaches indicating an increase in photon energy absorption with higher Bi_2O_3 content. This trend aligns with the known high mass attenuation coefficient of Bi_2O_3 and its dense atomic structure, as reported by Recep [41] for similar glass compositions. By increasing the Bi_2O_3 amount in the glass's composition from the GSB2 glass to the GSB2-15 glass, photon energy absorption is enhanced because of the high mass attenuation coefficient and high ratio of atomic weight to the atomic radius of the bismuth and dense spatial arrangement, which lead to dense structure glass creation.

3.4.2. Radiation absorption simulation of the glasses by the XCOM program

When rays collide with absorbent material due to collisions with electrons and absorbent object atoms, the output beam reduces. This reduction depends on the number of electrons in the absorber layer. The mass attenuation coefficient (μ/ρ) is a normalization of the linear attenuation coefficient per unit density of a material producing a value that is constant for a given element or compound so it is independent of the density of the material, and it is a fraction of photons that decreases when passing through the material.

XCOM, developed by Berger and Hubbell, is used to calculate mass attenuation coefficients for energies ranging from 1 keV to 100 GeV [42]. Hakan et al. [43] utilized XCOM to determine the mass attenuation coefficients of alloy powder and assess its radiation shielding properties.

The mass attenuation coefficient is the total of the photoelectric absorption, Compton phenomenon, and pair production effects. In the gamma-ray energy, three primary processes—atomic photoelectric effect, Compton (incoherent) scattering, and pair production—are the principal modes of interaction with materials [44]. Fig. 12 shows the atomic absorption coefficient based on photon energy diagrams for the glasses containing the Bi_2O_3 additive from 0 to 15 mol%. Compton absorption is independent of the atomic number and relates to the number of electrons in each gram of material, and all four glasses almost have the same Compton absorption [45].

At low energy, photoelectric absorption is dominant to other phenomena, This dominance is because the probability of photoelectric interactions increases sharply as the photon energy decreases and is also highly dependent on the atomic number of the absorbing material [46]. Photoelectric absorption has been intensified by increasing the amount of Bi_2O_3 in the glass composition due to the increasing atomic number of the compound in energies lower than 662(Kev), and in this region of energy, the material absorbs radiation based on the photoelectric effect.

In energies higher than energy 1.02 (Mev), absorption occurs with pair production mechanisms in the electron and nuclear field, and it can be seen in Fig. 12. In energies higher than 50(Mev), pair production is the most important absorption factor.

In a broad sense, the mass attenuation coefficient exhibits an upward trend as the quantity of Bi_2O_3 is increased in the composition, rendering it particularly well-suited for applications in radiation shielding against high-energy radiation.

4. Conclusion

This study demonstrates the effectiveness of incorporating Bi_2O_3 into borosilicate glass for enhancing gamma radiation shielding properties. The GSB2-15 glass, containing 15 mol% Bi_2O_3, exhibits superior structural stability and radiation resistance, making it a promising candidate for protective applications. Increased Bi_2O_3 content improves photon energy absorption due to its high mass attenuation coefficient and denser glass structure. These findings contribute to the development of eco-friendly, lead-free materials for medical, nuclear, and aerospace shielding technologies.

CRediT authorship contribution statement

Mohammad Rezvani: Project administration, Investigation. **Hossein Javid Ghezelgechi:** Investigation.

Declaration of interest statement

We hereby declare that, we have no affiliations with or involvement in any organization or entity with any financial interest, or non-financial interest in subject matter or materials discussed in this manuscript.

References

[1] A.K.M. Reza Bagheri, Hassan Yousefnia, Gamma ray shielding study of barium–bismuth–borosilicate glasses as transparent shielding materials using MCNP-4C code, XCOM program, and available experimental data, Nucl. Eng. Technol. 49 (2017) 216–223.
[2] a J.L.a. Cherdsak Bootjomchai, Yenchai b Chadet, Raewat Laopaiboon, Gamma-ray shielding and structural properties of barium–bismuth–borosilicate glasses, Radiat. Phys. Chem. 81 (2012) 785–790.
[3] S.S. Ravneet Kaur, Om Prakash Pandey, FTIR structural investigation of gamma irradiated BaO–Na2O–B2O3–SiO2 glasses, Phys. B Condens. Matter 407 (2012) 4765–4769.
[4] Kayrat K. Kadyrzhanov, A.A. K, Marina Konuhova, Anatoli I. Popov, Dmitriy D. Shlimas, Daryn B. Borgekov, Determination of gamma radiation shielding efficiency by radiation-resistant composite ZrO2–Al2O3 – TiO2–WO3 – Nb2O5 ceramics, Opt. Mater. 154 (2024).
[5] Y.X. Daquan Shi, Yading Zhao, Xiaobing Ma, Jian Wang, Minghao Liu, Kunyang Yu, Evaluation of technical and gamma radiation shielding properties of sustainable ultra-high performance geopolymer concrete, Constr. Build. Mater. 436 (2024).
[6] H.E. Yusuf Kavun, Kerli Suleyman, Mustafa Kavgac, Fabrication and characterization of GdxFe2O3(100-x)/PVA (x=0, 5, 10, 20) composite films for radiation shielding, Appl. Radiat. Isot. 177 (2021).
[7] D.S. Preet Kaur, Tejbir Singh, Heavy metal oxide glasses as gamma rays shielding material, Nucl. Eng. Des. 307 (2016) 364–376.

[8] A. El-Sayed, M.A.F. Waly, Mohamed A. Bourham, Gamma-ray mass attenuation coefficient and half value layer factor of some oxide glass shielding materials, Ann. Nucl. Energy 96 (2016) 26–30.
[9] B.A. Kaan Dogru, Abuzer Acikgoz, Demet Yilmaz, Abdul Fatah Pathman, Serife Yalcin, Gokhan Demircan, Structural, thermal, and radiation shielding properties of B2O3-TeO2-Bi2O3-CdO-Tm2O3 glasses: the role of Tm2O3, Ceram. Int. 50 (2024) 47384–47394.
[10] B.A. Burak Berke Solak, Demet Yilmaz, Sedanur Kalecik, Serife Yalcin, Abuzer Acikgoz, Gokhan Demircan, Exploring the radiation shielding properties of B2O3-PbO-TeO2-CeO2-WO3 glasses: a comprehensive study on structural, mechanical, gamma, and neutron attenuation characteristics, Mater. Chem. Phys. (2024) 312.
[11] W.E. Lee, M.I.O., Fundamentals of radioactive waste (RAW): science, sources, classification and management strategies, Radioactive Waste Management and Contaminated Site Clean-Up Processes (2013) 3–49.
[12] N. Chanthima, J. K, P. Limkitjaroenporn, S. Tuscharoen, Development of BaO–ZnO–B2O3 glasses as a radiation shielding material, Radiat. Phys. Chem. 137 (2017) 72–77.
[13] R. El-Mallawany, The Physics of Advanced Optical Materials: Tellurite Glasses, Springer, Cham, 2024.
[14] N. Elkhoshkhany, R. A, R. El-Mallawany, S.F. Hathot, Optical properties and crystallization of bismuth boro-tellurite glasses, J. Non-Cryst. Solids 476 (2017) 15–24.
[15] Z.W. Shufeng Song, Yu Liu, The effect of substitution of Bi2O3 for alkali oxides on thermal properties, structure and wetting behavior of the borosilicate glass, Mater. Lett. 64 (2010) 1025–1027.
[16] G.B.b. Ghada Almisned a, c Duygu Sen Baykal, T. Fatema, Ali d, G. Kilic e, H. O, Tekin *Bismuth(III) oxide and boron(III) oxide substitution in bismuth-boro-zinc glasses: a focusing in nuclear radiation shielding properties*, Optik 272 (2023).
[17] K. Kirdsiri, J. K, W. Chewpraditkul, P. Limsuwan, Photon interaction in borate glass system containing Bi2O3, PbO and BaO at 60 keV: theoretical calculation, Adv. Mater. Res. 93–94 (2010) 9–12.
[18] N. Chanthima, J. K, Influence of Bi2O3 on borophosphate glasses properties, Adv. Mater. Res. 979 (2014) 343–346.
[19] K. El-Egili, Infrared studies of Na2O–B2O3–SiO2 and Al2O3–Na2O–B2O3–SiO2 glasses, Phys. B Condens. Matter 325 (2003) 340–348.
[20] D. Ehrt, W.V., Radiation effects in glasses, Nucl. Instrum. Methods Phys. Res. Sect. B Beam Interact. Mater. Atoms 65 (1992) 1–8.
[21] Y.R. Akshatha Wagh, Vyasa Upadhyaya, Sudha D. Kamath, Composition dependent structural and optical properties of PbF2–TeO2–B2O3–Eu2O3 glasses, Spectrochim. Acta Mol. Biomol. Spectrosc. 151 (2015) 696–706.
[22] M. Mariyappan, K. M, M.I. Sayyed, M.G. Dong, U. Kara, Effect Bi2O3 on the physical, structural and radiation shielding properties of Er3+ ions doped bismuth sodiumfluoroborate glasses, J. Non-Cryst. Solids 499 (2018) 75–85.
[23] K.J.S. Kulwinder Kaur, Vikas Anand, Structural properties of Bi2O3–B2O3–SiO2–Na2O glasses for gamma ray shielding applications, Radiat. Phys. Chem. 120 (2016) 63–72.
[24] A. Rahman, G. M, E. Cattaruzza, F. Gonella, A. Quaranta *Glass structure modifications induced by diffusion of chromium ions into silicate glasses: An investigation by in-depth profiling Raman micro-spectroscopy*, Solid State Ionics 230 (2013) 59–65.
[25] A.M. Abdelghany, Novel method for early investigation of bioactivity in different borate bio-glasses, Spectrochim. Acta Mol. Biomol. Spectrosc. 100 (2013) 120–126.
[26] S. Sindhu, S. S, S. Rani, A. Agarwal, V.P. Seth, Modification of structure and electrical conductivity of cadmium borate glasses in the presence of V2O5, Mater. Chem. Phys. 107 (2008) 236–243.
[27] M.S. Gaafar, S.Y. M, Mechanical and structural studies on sodium borosilicate glasses doped with Er2O3 using ultrasonic velocity and FTIR spectroscopy, Phys. B Condens. Matter 388 (2007) 294–302.
[28] E.I. Kamitsos, A.P. P, M.A. Karakassides, G.D. Chryssiko, Infrared reflectance spectra of lithium borate glasses, J. Non-Cryst. Solids 126 (1990) 52–67.
[29] E.I. Kamitsos, M.A. K, A.P. Patsis, Spectroscopic study of carbonate retention in high-basicity borate glasses, J. Non-Cryst. Solids 111 (1989) 252–262.
[30] R. Iordanova, V. D, Y. Dimitriev, D. Klissurski, Glass formation and structure of glasses in the V2O5·MoO3·Bi2O3 system, J. Non-Cryst. Solids 180 (1994) 58–65.
[31] A. Bishay, H. El Lozy, Electron spin resonance studies of some irradiated alkali borate glasses containing trivalent cerium, Non-Crystalline Solids 1 (1969) 437–440.
[32] A. David, I.S.M. McKeown, Andrew C. Buechele, Ian L. Pegg, Christopher A. Kendziora, Structural characterization of high-zirconia borosilicate glasses using Raman spectroscopy, J. Non-Cryst. Solids 262 (2000) 126–134.
[33] Z.H. Feng He, Junlin Xie, Yuhui Li, IR and Raman spectra properties of Bi2O3-ZnO-B2O3-BaO quaternary glass system, Am. J. Anal. Chem. 5 (2014) 8.
[34] W.G.O. Fan Piao, Eugene E. Haller, The mechanism of radiation-induced compaction in vitreous silica, J. Non-Cryst. Solids 276 (2000) 61–71.
[35] Feng He, Caiming Ping, Yuanyuan Zheng, Viscosity and structure of lithium sodium borosilicate glass, Phys. Procedia 48 (2013) 73–80.
[36] C. Gautam, A.K. Yadav, A.K. Singh, A review on infrared spectroscopy of borate glasses with effects of different additives, ISRN Ceramics 2012 (2012) 428497.
[37] A.M. Abdelghany, F.H. E, H.A. ElBatal, F.M. EzzElDin, Optical and FTIR structural studies of CoO-doped sodium borate, sodium silicate and sodium phosphate glasses and effects of gamma irradiation-a comparative study, J. Mol. Struct. 1074 (2014) 503–510.
[38] A. Abdeldaym, O.I. S, F.M. Ezz-Eldin, N.A. Elalaily, Influence of gamma irradiation on the optical, thermal and electrical features of blue commercial glass as potential accident dosimetry, J. Phys. Chem. Solid. 157 (2021).
[39] M.H.A.M. Awatif Alshamari, N. Alonizan, Nidal Dwaikat, Ibrahim Alrammah, Mohammed Alsuhybani, Q.A. Drmosh, Influence of various gamma-ray doses on radiation shielding, thermal, mechanical, structural, and optical properties of tellurite, borate, and boro-tellurite glasses modified with molybdenum and strontium oxide, Opt. Mater. 142 (2023).
[40] H.A. ElBatal, A.M. A, I.S. Ali, Optical and FTIR studies of CuO-doped lead borate glasses and effect of gamma irradiation, J. Non-Cryst. Solids 358 (2012) 820–825.
[41] T.K. Recep Kurtulus, Iskender Akkurt, Kadir Gunoglu, H.O. Tekin, Cansu Kurtulus, A comprehensive study on novel alumino-borosilicate glass reinforced with Bi2O3 for radiation shielding applications: synthesis, spectrometer, XCOM, and MCNP-X works, J. Mater. Sci. Mater. Electron. 32 (2021) 13882–13896.
[42] L. Gerward, N. G, K.B. Jensen, H. Levring, WinXCom—a program for calculating X-ray attenuation coefficients, Radiat. Phys. Chem. 71 (2004) 653–654.
[43] H.E. Hakan Yaykaslı, Yusuf Kavun, Musa Gogebakan, Microstructural, thermal, and radiation shielding properties of Al50B25Mg25 alloy prepared by mechanical alloying, J. Mater. Sci. Mater. Electron. 33 (2022) 2350–2359.
[44] S. Prasanna Kumar a, T.K. U, Effective atomic number of composite materials for Compton effect in the gamma ray region 280–1115 keV, Appl. Radiat. Isot. 68 (2010) 2443–2447.
[45] P.G.R. Claude Leroy, Principles of Radiation Interaction in Matter and Detectio, third ed., World Scientific Publishing Co, 2009.
[46] R.H. Pratt, Photon absorption and photon scattering—what we do not know and why it matters, Radiat. Phys. Chem. 95 (2014) 4–13.